Chemical Science

ROYAL SOCIETY OF CHEMISTRY

EDGE ARTICLE

View Article Online
View Journal | View Issue

Cite this: *Chem. Sci.*, 2020, **11**, 5082

All publication charges for this article have been paid for by the Royal Society of Chemistry

Synthesis and properties of hypervalent electron-rich pentacoordinate nitrogen compounds†

Chenting Yan, [a] Masato Takeshita,[a] Jun-ya Nakatsuji,[a] Akihiro Kurosaki,[a] Kaoko Sato,[a] Rong Shang, *[a] Masaaki Nakamoto,[a] Yohsuke Yamamoto, *[a] Yohei Adachi, [b] Ko Furukawa,[c] Ryohei Kishi[d] and Masayoshi Nakano [de]

Received 1st January 2020
Accepted 8th April 2020

DOI: 10.1039/d0sc00002g

rsc.li/chemical-science

Isolation and structural characterization of hypervalent electron-rich pentacoordinate nitrogen species have not been achieved despite continuous attempts for over a century. Herein we report the first synthesis and isolation of air stable hypervalent electron-rich pentacoordinate nitrogen cationic radical (**11-N-5**) species from oxidation of their corresponding neutral (**12-N-5**) species. In the cationic radical species, the nitrogen centers adopt a trigonal bipyramidal geometry featuring a 3-center-5-electron hypervalent attractive interaction. The combination of single crystal X-ray diffraction analysis and computational studies revealed weak N–O interactions between the central nitrogen cation and oxygen atoms. This successful design strategy and isolation of air-stable pentacoordinate hypervalent nitrogen species allow further investigations on reactivity and properties resulting from these unusually weakly coordinating interactions in nitrogen compounds.

1 Introduction

Hypervalent compounds[1,2] have been defined as main group element compounds which contain a number of formally assignable electrons of more than the octet in a valence shell directly associated with the central atom.[1,3,4] More recently, Parkin[5] clearly distinguished main group element compounds that feature three-center four-electron (3c-4e) interactions from those that feature 3c-2e interactions. The former, in which one of the atoms appears to have an expanded octet, are termed "*electron-rich*" hypervalent molecules. The latter are invoked for so-called "*electron deficient*" hypercoordinate molecules.[6–14]

The *N*-X-*L* nomenclature[15] has been used to classify hypervalent compounds, where *N* is the number of valence electrons formally present on the central element according to the Lewis diagram, X is the identity of the central element and *L* is the number of ligand atoms bonded to the central atom. Parkin proposed $ML_lX_xZ_zH_h$ classifications,[5] which are more detailed descriptions of the *N*-X-*L* nomenclature.

The debate on the fundamental bonding descriptions of this class of compounds to understand why they do not comply to the Lewis "octet rule" has lasted for decades on the theoretical front.[4,7–10,16–27] In a recent review, Crabtree[28] pointed out the similarity among hypervalency and other types of weak bonding and the valence shell of the central atom is essentially an octet and the electrons beyond 8e are predominantly located on ligands, not on the central atom. The hypervalent bonding nature and geometry have significant implications in several current fast-growing areas of synthetic organic chemistry, such as hypervalent iodine reagents,[29–31] sterically constrained T-shaped phosphorus(III) compounds in small molecule activation and catalysis,[32–39] and application of new heavier group 14 [40] and 15 [41–47] Lewis acids in frustrated Lewis pair chemistry. While hypervalent compounds of heavy main group elements are common,[2,47–53] those of the light, second row elements still remain a synthetic challenge, with only a handful of isolated and structurally confirmed examples of penta-/hexa-coordinate carbon[54–57] and boron[58–61] compounds reported (Chart 1B and C).

Hypervalent pentacoordinate nitrogen species (**10-N-5**) are some of the most fundamental hypervalent compounds, with their synthetic attempts traced back to 1916.[62–70] Despite theoretical calculations predicting their existence and structural stability,[71–76] thermally stable hypervalent nitrogen compounds (*N*–N–*L*; $N > 10$, $L > 4$) have not been reported to date.[68,70,77,78] Some success has been achieved by detection,[79–83] isolation and

[a]*Department of Chemistry, Graduate School of Science, Hiroshima University, 1-3-1 Kagamiyama, Higashi-Hiroshima 739-8526, Japan. E-mail: yohsuke@hiroshima-u.ac.jp; rshang@hiroshima-u.ac.jp*

[b]*Department of Applied Chemistry, Graduate School of Engineering, Hiroshima University, 1-3-1 Kagamiyama, Higashi-Hiroshima 739-8526, Japan*

[c]*Center for Coordination Research Facilities, Institute for Research Promotion, Niigata University, 8050 Ikarashi 2-no-cho, Nishi-ku, Niigata 950-2181, Japan*

[d]*Department of Materials Engineering Science, Graduate School of Engineering Science, Osaka University, Toyonaka, Osaka 560-8531, Japan*

[e]*Department of Materials Engineering Science, Graduate School of Engineering Science, Osaka University, Toyonaka, Osaka 560-8531, Japan*

† Electronic supplementary information (ESI) available: Synthetic and computational details, X-ray crystallographic data and NMR spectra. CCDC 1945530–1945536, 1988910. For ESI and crystallographic data in CIF or other electronic format see DOI: 10.1039/d0sc00002g

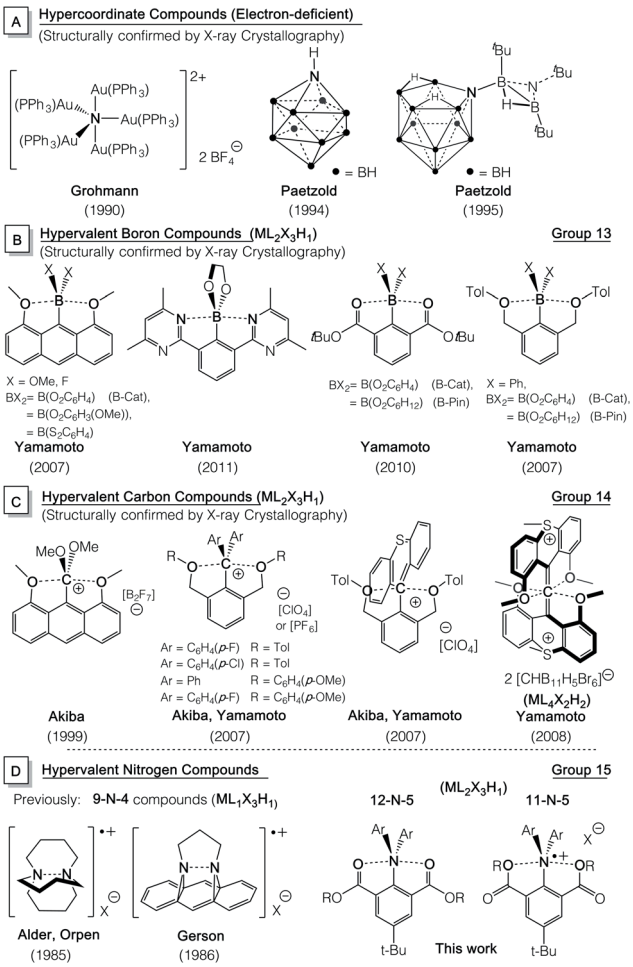

Chart 1 Structurally confirmed hypercoordinate (A) nitrogen and hypervalent (B) boron, (C) carbon and (D) nitrogen compounds.

structural characterization of transient, as well as stable[84–86] hypervalent tetracoordinate nitrogen radical species (**9-N-4**, Chart 1D).

Here we report the first hypervalent "*electron-rich*" pentacoordinate nitrogen cationic radical (**11-N-5** or $\mathbf{ML_2X_3H_1}$) species with 3c-5e interactions and their corresponding neutral (**12-N-5**) compounds although "*electron-deficient*" pentacoordinate nitrogen compounds[6–9,87,88] have been reported as shown in Chart 1A.

2 Results and discussion

To stabilize the trigonal-bipyramidal (TBP) geometry of a **10-N-5** structure, which is typically a transition state resembling an S_N2 reaction,[1,3] we targeted the tridentate 2,6-di(alkoxycarbonyl) phenyl framework[60] in consideration of two crucial factors: (i) electronegative elements (oxygen) are positioned at apical positions to localize the electron density at the 3-center-4-electron (3c-4e) hypervalent bond and (ii) the apical 3c-4e attractive interaction should be weak enough (O···N attractive interactions) to avoid a "bell-clapper" type equilibrium.[89,90] The alkoxycarbonyl groups provide some degree of steric rigidity, which plays an important role in balancing the two factors and thus stabilizing the hypervalent compounds. The *tert*-butyl group at the *para* position increases the solubility.

We synthesized neutral triarylamine precursors $\mathbf{2^{Me}a\text{-}b}$ and $\mathbf{2^{iPr}a\text{-}b}$ from the Ullmann coupling reaction of methoxyl- and isopropoxyl-carbonyl substituted bromobenzenes ($\mathbf{1^{Me}}$ and $\mathbf{1^{iPr}}$) with chloro- and trifluoromethyl-substituted diarylamines (Scheme 1). Compounds $\mathbf{2^{Me}a\text{-}b}$ and $\mathbf{2^{iPr}a\text{-}b}$ were isolated as white to pale yellow solids and found fluorescent in solution. Their absorption spectra obtained in CH_2Cl_2 showed two absorption bands at approximately 310 nm and 350 nm, which are assignable to HOMO–LUMO+2 and HOMO–LUMO transitions, respectively (Fig. S7†). The similar absorption wavelengths and oscillator strengths between methyl- and isopropyl-substituted analogues suggest very similar electronic structures of $\mathbf{2^{Me}a\text{-}b}$ and $\mathbf{2^{iPr}a\text{-}b}$ in their ground state. In contrast to the similarities of absorption, the fluorescence emission of $\mathbf{2^{Me}a\text{-}b}$ and $\mathbf{2^{iPr}a\text{-}b}$ measured in CH_2Cl_2 at 25 °C showed substituent-dependence on the aryl groups (X = Cl or CF_3, see Fig. S1 and Table S1†). The ester groups (R = Me or i-Pr) do not exert clear influence. The quantum yields of $\mathbf{2^{iPr}a\text{-}b}$ (9.43%, 13.95% respectively) with R = i-Pr are obviously higher than those of $\mathbf{2^{Me}a\text{-}b}$ (3.22%, 3.50% respectively) with R = Me, likely due to the more restricted rotation around the N-Ph bonds with the sterically larger i-Pr groups.

Cyclic voltammetry (CV) of $\mathbf{2^{Me}a\text{-}b}$ and $\mathbf{2^{iPr}a\text{-}b}$ in CH_2Cl_2 at room temperature with $TBAPF_6$ as a supporting electrolyte revealed a reversible one electron oxidation wave at formal potentials of +1.196 V, +1.485 V, +1.177 V and +1.477 V *versus* Fc/Fc^+ respectively, indicating stability of the corresponding monocationic species (Fig. S3†). The σ withdrawing effect of trifluoromethyl groups is clearly shown in the higher oxidation potentials observed in $\mathbf{2^{Me}b}$ and $\mathbf{2^{iPr}b}$. The σ donating effect between the methyl and isopropyl substituents is much less prominent. A 2nd electron oxidation wave was not observed under this condition between −2.0 and 2.0 volts, which is the limit of our instrument.

The one electron oxidation reaction of $\mathbf{2^{Me}a\text{-}b}$ and $\mathbf{2^{iPr}a\text{-}b}$ (Scheme 2) was easily achieved by using 1 equiv. $(2,4\text{-}Br_2C_6H_3)_3NSbCl_6$ as an oxidant in CH_2Cl_2. Dark blue-green solids $\mathbf{3^{Me}a\text{-}b}$ and $\mathbf{3^{iPr}a\text{-}b}$ were obtained in moderate to high yields. The absorption spectra of $\mathbf{3^{Me}a\text{-}b}$ and $\mathbf{3^{iPr}a\text{-}b}$ showed bands at 600–800 nm, significantly red-shifted from those of the neutral

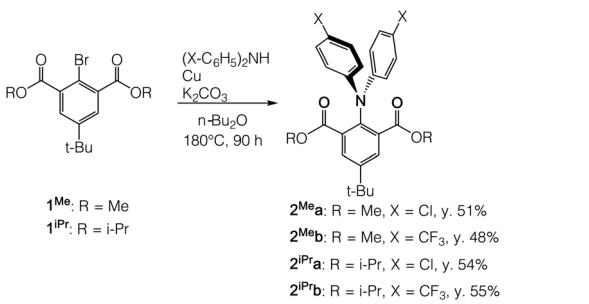

Scheme 1 Preparation of neutral triarylamine precursors 2^{Me}a-b and 2^{iPr}a-b.

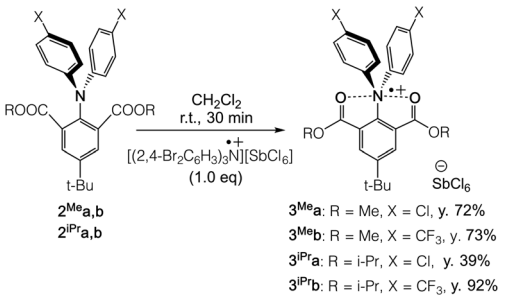

Scheme 2 One electron oxidation of 2^{Me}a-b and 2^{iPr}a-b.

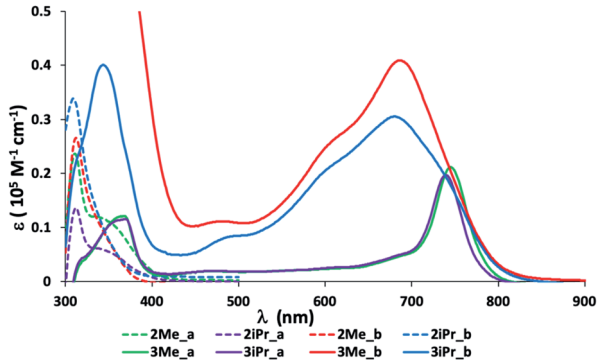

Fig. 1 Absorption spectra of 10^{-5} M 2^{Me}a-b and 2^{iPr}a-b (dashed line) and 3^{Me}a-b and 3^{iPr}a-b (solid line) in CH_2Cl_2 at 25 °C.

compounds in the visible region (*ca.* 310 nm, Fig. 1). This is due to the smaller HOMO–SOMO energy gaps of radical species in comparison to the HOMO–LUMO energy gaps in neutral species. The chloro-analogues 3^{Me}**a** (745 nm) and 3^{iPr}**a** (739 nm) showed absorption maxima at noticeably longer wavelengths compared to their CF_3-substituted 3^{Me}**b** (688 nm) and 3^{iPr}**b** (681 nm), revealing that electron-donating substituents decrease HOMO–SOMO energy gaps. The chloro-substituted cationic radical species 3^{Me}**a** and 3^{iPr}**a** are stable in air and moisture for several days at room temperature without detectable decomposition. In contrast, the trifluoromethyl derivatives 3^{Me}**b** and 3^{iPr}**b** decompose readily when taken out of an inert atmosphere. All of them appear to be light-sensitive.

Single crystals suitable for X-ray crystallographic studies were obtained by recrystallization from CH_2Cl_2/hexane solution mixtures of 2^{Me}a-b, 2^{iPr}a-b, 3^{Me}**a** and 3^{iPr}**a** at room temperature. Their solid-state molecular structures and selected bonding parameters are shown in Fig. 2 and Table 1. Due to proneness to decomposition, publishable data of the trifluoromethyl-substituted derivatives 3^{Me}**b** and 3^{iPr}**b** could not be obtained. In all structures, the central nitrogen atoms are essentially planar, with the sum of the angles around nitrogen ($\sum N\alpha$) being larger than 359°. The ester groups seem to rotate along the carbon–carbon single bond, resulting in conformational differences between the solid-state structures of neutral (2^{Me}**a** and 2^{iPr}**a**) and oxidized compounds (3^{Me}**a** and 3^{iPr}**a**). The sp^3 alkoxyl oxygen (*O*R) atoms align almost coplanar with the central nitrogen atom in 2^{Me}**a** and 3^{iPr}**a**, while in the case of 2^{Me}**b**, 2^{iPr}**a-b** and 3^{Me}**a**, the sp^2 carbonyl (C*O*) oxygen atoms and the nitrogen atom are aligned. Calculations show that the energy differences resulting from the two coordination modes are trivial (<3 kcal mol^{-1}, see Table S12 and Fig. S15†). Therefore, conformational preferences observed in the crystals may be influenced significantly by crystal packing energy. This lack of consistency of coordination modes makes the structural comparison difficult to elucidate.

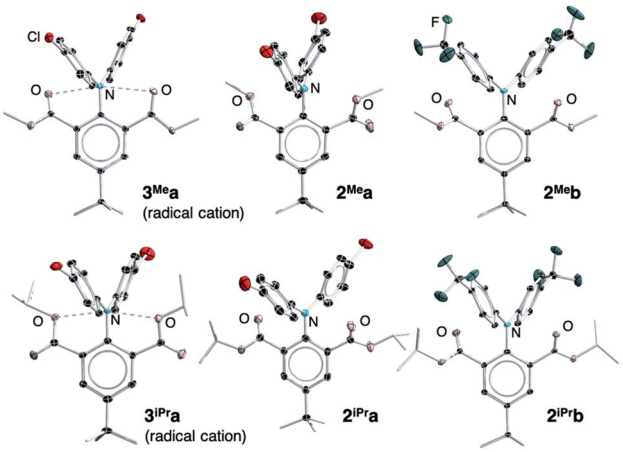

Fig. 2 Solid-state molecular structures of 2^{Me}a-b, 2^{iPr}a-b, 3^{Me}**a** and 3^{iPr}**a**. Thermal ellipsoids are set at 30% probability. Ellipsoids of periphery atoms, hydrogen atoms, and counter ions are omitted for clarity. A side-view is included in the ESI.† CCDC numbers: 1945530–1945536.[91]

In all the structures, the ester groups twist out of the plane of their attached phenyl ring (Fig. S5† for a side view). Although the N–O bond lengths in all neutral and cationic species are longer than the sum of the covalent bond radii of N and O atoms (1.34 Å),[92] they are shorter than the sum of van der Waals radii of N and O atoms (2.79–3.16 Å),[93–99] falling in the upper range of previously reported hypervalent bonds.[56] This suggests possible weak interactions between the central nitrogen atom and both oxygen atoms in both cationic and neutral structures. The torsion angles (Φ) between CO1 and CO2 (Table 1) are the smallest in the formally **11-N-5** cationic species 3^{Me}**a** and 3^{iPr}**a** (47.7° and 49.0° respectively). They correspond to the shortest N–O distances, 2.721(3) Å and 2.790(3) Å (3^{Me}**a**) and 2.662(5) Å, 2.676(5) Å (3^{iPr}**a**) among all structures, indicating the strongest N–O interactions.

Among the neutral compounds, the trend of torsion angles (Φ_{occo}) correlate with that of N–O distances, increasing from 2^{Me}**a** (2.793(18) Å, 77.8°) and 2^{iPr}**b** (2.855(13) Å, 77.3°) to 2^{iPr}**a** (2.921(3) Å, 81.9°) and lastly, 2^{Me}**b** (2.980(16) Å, 90.7°). These N–O distances are slightly shorter than those in Shimizu and co-worker's parent 2-aminoisophthalic acid diester, $Ph_2N[C_6H_3$(-COOMe)] (3.093 Å and 2.984 Å), which also displayed a larger Φ_{occo} (96.6°).[100]

As an additional comparison, we investigated the molecular structure of the bromo-substituted starting material 1^{Me}, which may not be expected to form the same type of pentacoordinate hypervalent interaction. (Fig. S4†). The smallest Φ_{occo} of 120.4°

Table 1 Selected experimental bond lengths (Å), angles and dihedral angles [°] of 2^{Me}a-b, 2^{iPr}a-b, 3^{Me}a and 3^{iPr}a

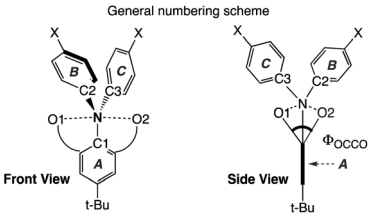

	Ionic radical	Neutral		Ionic radical	Neutral	
Parameters	3^{Me}a	2^{Me}a	2^{Me}b	3^{iPr}a	2^{iPr}a	2^{iPr}b
Coord.	(C***O***)	(***O***Me)	(C***O***)	(***O***iPr)	(C***O***)	(C***O***)
N–O1	2.721(3)	2.764(18)	2.945(15)	2.662(5)	2.891(3)	2.843(12)
N–O2	2.790(3)	2.823(18)	3.015(16)	2.676(5)	2.952(3)	2.868(13)
N–O_{Ave}	2.755(3)	2.793(18)	2.980(16)	2.669(5)	2.921(3)	2.855(13)
N–C1	1.440(3)	1.423(2)	1.422(18)	1.454(6)	1.409(5)	1.428(12)
N–C2	1.376(3)	1.408(2)	1.411(17)	1.383(5)	1.408(5)	1.405(13)
N–C3	1.409(3)	1.414(2)	1.415(17)	1.397(6)	1.420(5)	1.404(14)
Σ$N\alpha$	360.0(6)	359.1(39)	359.8(31)	359.9(12)	359.5(9)	360.0(24)
Φ_{OCCO}	47.7	77.8	90.7	49.0	81.9	77.3

in $\mathbf{1}^{Me}$ is much larger than those found in our neutral compounds (2^{Me}**a-b** and 2^{iPr}**a-b**) formed from the methoxy group on each side of the bromo-substituent. This shows that there is no preferred alignment of the two ester groups of $\mathbf{1}^{Me}$ through C_{phenyl}-C_{ester} rotation for a small Φ_{occo} in the absence of the 3c-5e attractive interaction.

Overall, in the solid state, sp^3 alkoxyl (*OR*) coordination forms shorter apical N–O interactions and thus stronger attractive interaction than those from the sp^2 carbonyl (C***O***) coordination. In addition, the N–O interactions are stronger in cationic radical species than those in neutral compounds.

To confirm the interactions between the central nitrogen atom and the two oxygens in both neutral and cationic radical species, DFT calculations were carried out at the RCAM-B3LYP-D3/def2-SVP level for **2** and at the UCAM-B3LYP-D3/def2-SVP level for **3** using the Gaussian 09 program (Table S6†). The optimized structures corroborate well with the crystal structures except 2^{Me}**b**, in which the N–O distances are underestimated.[101] The unsystematic inconsistency between calculated and solid-state structures may be due to the solvent effect during the recrystallization process and packing effect of the crystal. Therefore, Atoms in Molecules (AIM) analysis of 2^{Me}**a-b**, 2^{iPr}**a-b**, 3^{Me}**a** and 3^{iPr}**a** was carried out based on single point calculations of the X-ray geometries (Fig. 3 and Table S10†).[102]

The results of the cation radical species (3^{Me}**a** and 3^{iPr}**a**) showed (3, −1) critical points between the central nitrogen atom and the ester oxygen atoms with small electron densities ($\rho(r)$ 0.014–0.017 e/a_o^3) and small positive Laplacian values ($\nabla^2\rho(r)$ 0.051–0.064 e/a_o^5). This indicates that the N–O interactions in 3^{Me}**a** and 3^{iPr}**a** are weak and polarized, similar to those of the reported second row hypervalent compounds ($\rho(r)$, 0.014 – 0.022 e/a_o^3 and $\nabla^2\rho(r)$, 0.051–0.078 e/a_o^5).[54–57]

According to the review paper by A. C. Tsipis,[103] the following classifications are presented based on the character of the bond/interaction:

(1) $\nabla^2\rho < 0$ and $H_{cp} < 0$ indicate weakly polar and nonpolar covalent bonds.

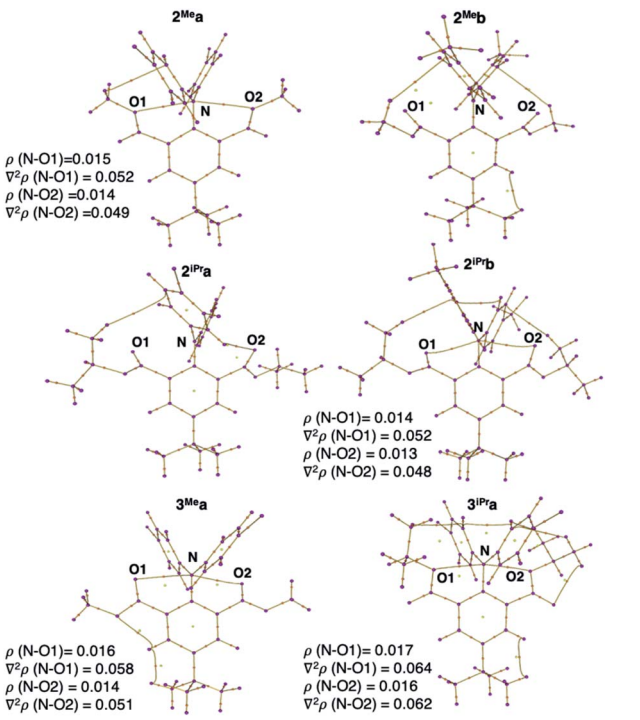

Fig. 3 Atom in molecules (AIM) analysis results based on X-ray geometries of 2^{Me}a-b, 2^{iPr}a-b, 3^{Me}a and 3^{iPr}a showing bond paths between the central nitrogen and the carbonyl oxygen, calculated at the RCAM- and UCAM-B3LYP-D3/def2-SVP levels in **2** and **3**, respectively.

(2) $\nabla^2\rho > 0$ and $H_{cp} < 0$ correspond to intermediate interactions including strong hydrogen bonds and most of the coordination bonds.

(3) $\nabla^2\rho > 0$, $\rho(r) < 0.2$ and $G_{cp}/\rho_{cp} > 1$ indicate closed-shell interactions such as weak hydrogen bonds and van der Waals interactions.

(4) $\nabla^2\rho > 0$ and $|V_{cp}|/G_{cp} < 1$ characterize ionic bonding.

The AIM results of $\mathbf{3^{Me}a}$ and $\mathbf{3^{iPr}a}$ (Table S10†) match the criteria of the class **3** and **4** mostly, which revealed an ionic (non-covalent), weak secondary bonding nature of the N–O interactions. This provides further support for Crabtree's generalization of hypervalent, hydrogen and secondary bonding interactions.[28]

Among neutral species, although no hypervalent bonding was expected due to the repulsion between the nitrogen and oxygen lone pairs, the AIM analysis showed (3 −1) critical points between N and O atoms in $\mathbf{2^{Me}a}$ and $\mathbf{2^{iPr}b}$. Their electron density (0.013–0.015 e/a_o^3) and Laplacian (0.048–0.052 e/a_o^5) values are slightly smaller than those found in cationic species ($\rho(r)$ 0.014–0.017 e/a_o^3, $\nabla^2\rho(r)$ 0.051–0.064 e/a_o^5). In contrast, no N–O (3, −1) critical points were found in $\mathbf{2^{Me}b}$ and $\mathbf{2^{iPr}a}$ (Fig. 3). These AIM results corroborates well with the N–O distances: cation radicals show the shortest N–O distances (2.662–2.790 Å) and (3, −1) critical points with the highest $\rho(r)$ and $\nabla^2\rho(r)$ values, followed by $\mathbf{2^{Me}a}$ and $\mathbf{2^{iPr}b}$ with intermediate N–O distances (2.764–2.868 Å) and weaker (3, −1) critical points. The N–O distances in $\mathbf{2^{Me}b}$ and $\mathbf{2^{iPr}a}$ are the longest (2.891–3.015 Å) and no (3, −1) critical points were found along the N–O paths.

Combined X-ray bonding analysis and theoretical AIM studies suggest that the N–O interactions in the cation radical cases are stronger than in the neutral cases. $\mathbf{3^{Me}a}$ and $\mathbf{3^{iPr}a}$ should be regarded as hypervalent electron-rich pentacoordinate nitrogen species with a 3c-5e attractive interaction ($\mathbf{ML_2X_3H_1}$). The neutral compounds may or may not exert weak N–O attractive interactions. Any N–O interactions exhibited in the neutral case may originate from the effective delocalization of the nitrogen electron lone pair in the triarylamine structure (evident by the planar amine geometry and slightly shortened N–C_{ipso} bond distances, Table 1). The slightly positive nitrogen atom then can form electrostatic interactions with the adjacent oxygen electron pairs, forming an $n_O \rightarrow \pi^*_{NC}$ interaction (Fig. 4).

The cationic radical compounds $\mathbf{3^{Me}a\text{-}b}$ and $\mathbf{3^{iPr}a\text{-}b}$ were also characterized by Electron Paramagnetic Resonance (EPR) spectroscopy in CH_2Cl_2 (Fig. 5). In all cases, the spectrum showed a nitrogen centered radical with hyperfine coupling to hydrogen nuclei of the singly substituted aryl groups (rings ***B*** and ***C***, Table 1), indicating that the radical delocalizes over the aryl groups ***B*** and ***C*** in all structures (Table S3 and Fig. S9–S12†). Larger hyperfine coupling constants (A_{H1} and A_{H2}) in rings ***B*** and ***C*** and additional coupling contribution from the heteroatoms (Cl and F) were observed. This suggests that stronger electron-withdrawing CF_3-substituents promote delocalization of the radical in the structures. The delocalization to the phenyl rings ***B*** and ***C*** is more effective than ***A***, reflected by the significantly longer N–C1 distances in comparison to N–C2/C3 distances in the solid-state structures of $\mathbf{3^{Me}a}$ and $\mathbf{3^{iPr}a}$ (Table 1).

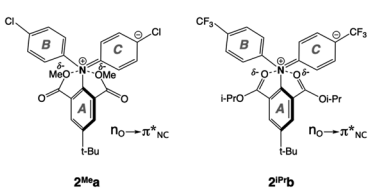

Fig. 4 The delocalization structures of neutral compounds ($\mathbf{2^{Me}a}$ and $\mathbf{2^{iPr}b}$) with electron-withdrawing groups (-Cl and CF_3).

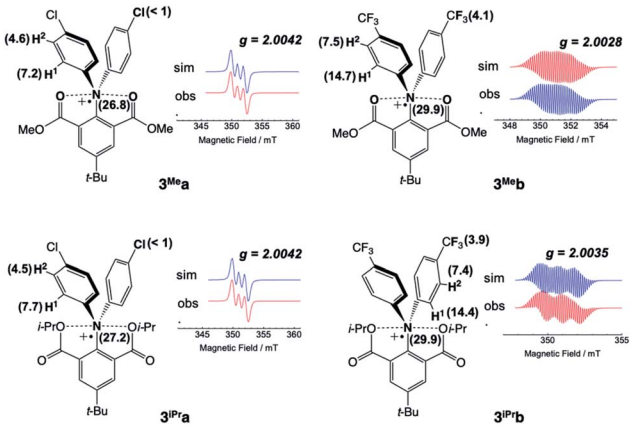

Fig. 5 Observed (bottom) and simulated (top) EPR spectra of $\mathbf{3^{Me}a\text{-}b}$ and $\mathbf{3^{iPr}a\text{-}b}$ in CH_2Cl_2 solution at 25 °C. Spin Hamiltonian parameters estimated from simulation are labelled in MHz (Table S3†).

3 Conclusions

In conclusion, we successfully synthesized, isolated, and structurally characterized the first air stable hypervalent "electron-rich" pentacoordinate nitrogen compounds. The N–O bond distance in cationic radical species is shorter than the sum of N–O van der Waals radii, indicating attractive interactions between N and O atoms. AIM calculations showed the presence of (3, −1) critical points along the N–O bond paths in cationic radical species, confirming the formation of **11-N-5** hypervalent 3c-5e bonding. In addition, the shorter N–O bond distances and the presence of (3, −1) critical points in neutral compounds $\mathbf{2^{Me}a}$ and $\mathbf{2^{iPr}b}$ suggest possible electrostatic **12-N-5** interactions, likely due to an $n_O \rightarrow \pi^*_{NC}$ stabilization effect.

The isolation of these new nitrogen compounds and confirmation of their weak attractive interaction will allow us to explore the effect of weak electronic perturbation on the properties and/or reactivity of nitrogen containing compounds.

Conflicts of interest

There are no conflicts to declare.

Acknowledgements

The authors thank Prof. Joji Ohshita and Prof. Kenji Komaguchi for the use of their instruments and discussion. This work was

supported by the JSPS KAKENHI Grant (24109002) from the Ministry of Education, Culture, Sports, Science and Technology, Japan. The authors also thank Research Center for Computational Science (Okazaki, Japan) for the supercomputer time for theoretical calculations.

Notes and references

1 J. C. Martin, *Science*, 1983, **221**, 509–514.
2 K.-Y. Akiba, *Heteroat. Chem.*, 2011, **22**, 207–274.
3 J. I. Musher, *Angew. Chem., Int. Ed.*, 1969, **8**, 54–68.
4 W. B. Jensen, *J. Chem. Educ.*, 2006, **83**, 1751.
5 M. L. Green and G. Parkin, *Dalton.Trans.*, 2016, **45**, 18784–18795.
6 A. Grohmann, J. Riede and H. Schmidbaur, *Nature*, 1990, **345**, 140–142.
7 G. A. Olah, A. M. White and D. H. O'Brien, *Chem. Rev.*, 1970, **70**, 561–591.
8 G. A. Olah and G. Rasul, *Acc. Chem. Res.*, 1997, **30**, 245–250.
9 P. v. R. Schleyer, E. U. Wuerthwein, E. Kaufmann, T. Clark and J. A. Pople, *J. Am. Chem. Soc.*, 1983, **105**, 5930–5932.
10 H. Kudo, *Nature*, 1992, **355**, 432–434.
11 P. v. R. Schleyer, B. Tidor, E. D. Jemmis, J. Chandrasekhar, E. U. Wuerthwein, A. J. Kos, B. T. Luke and J. A. Pople, *J. Am. Chem. Soc.*, 1983, **105**, 484–488.
12 Z. Varga, *Struct. Chem.*, 2017, **28**, 297–301.
13 W. Zhizhong, Z. Xiange and T. Auchin, *J. Mol. Struc.Theochem.*, 1998, **453**, 225–231.
14 R. D. Harcourt, *J. Organomet. Chem.*, 1994, **478**, 131–140.
15 C. W. Perkins, J. C. Martin, A. J. Arduengo, W. Lau, A. Alegria and J. K. Kochi, *J. Am. Chem. Soc.*, 1980, **102**, 7753–7759.
16 A. E. Reed and P. v. R. Schleyer, *J. Am. Chem. Soc.*, 1990, **112**, 1434–1445.
17 J. A. Dobado, H. Martínez-García, J. M. Molina and M. R. Sundberg, *J. Am. Chem. Soc.*, 1998, **120**, 8461–8471.
18 R. J. Gillespie and B. Silvi, *Coord. Chem. Rev.*, 2002, **233–234**, 53–62.
19 X. Sun, *Chem. Educat.*, 2002, **7**, 261–264.
20 S. Noury, B. Silvi and R. J. Gillespie, *Inorg. Chem.*, 2002, **41**, 2164–2172.
21 S. C. A. H. Pierrefixe, C. Fonseca Guerra and F. M. Bickelhaupt, *Chem. - Eur. J.*, 2008, **14**, 819–828.
22 P. G. Nelson, *Chem. Educ. Res. Prac.*, 2001, **2**, 67–72.
23 A. Kalemos, *J. Phys. Chem. A*, 2018, **122**, 2178–2183.
24 M. C. Durrant, *Chem. Sci.*, 2015, **6**, 6614–6623.
25 R. D. Harcourt and T. M. Klapötke, *Chem. Sci.*, 2016, **7**, 3443–3447.
26 M. C. Durrant, *Chem.Sci.*, 2016, **7**, 3448–3449.
27 S. C. A. H. Pierrefixe, S. J. M. van Stralen, J. N. P. van Stralen, C. Fonseca Guerra and F. M. Bickelhaupt, *Angew. Chem., Int. Ed.*, 2009, **48**, 6469–6471.
28 R. H. Crabtree, *Chem. Soc. Rev.*, 2017, **46**, 1720–1729.
29 A. Yoshimura and V. V. Zhdankin, *Chem. Rev.*, 2016, **116**, 3328–3435.
30 A. Yoshimura, M. S. Yusubov and V. V. Zhdankin, *Org. Biomol. Chem.*, 2016, **14**, 4771–4781.
31 L. Catalano, G. Cavallo, P. Metrangolo, G. Resnati and G. Terraneo, *Top. Curr. Chem.*, 2016, **373**, 289–310.
32 E. E. Coyle and C. J. O'Brien, *Nat. Chem.*, 2012, **4**, 779.
33 M. Driess, N. Muresan, K. Merz and M. Päch, *Angew. Chem., Int. Ed.*, 2005, **44**, 6734–6737.
34 S. A. Culley and A. J. Arduengo, *J. Am. Chem. Soc.*, 1984, **106**, 1164–1165.
35 A. J. Arduengo, C. A. Stewart, F. Davidson, D. A. Dixon, J. Y. Becker, S. A. Culley and M. B. Mizen, *J. Am. Chem. Soc.*, 1987, **109**, 627–647.
36 A. J. Arduengo and C. A. Stewart, *Chem. Rev.*, 1994, **94**, 1215–1237.
37 N. L. Dunn, M. Ha and A. T. Radosevich, *J. Am. Chem. Soc.*, 2012, **134**, 11330–11333.
38 T. P. Robinson, D. M. De Rosa, S. Aldridge and J. M. Goicoechea, *Angew. Chem., Int. Ed.*, 2015, **54**, 13758–13763.
39 W. Zhao, S. M. McCarthy, T. Y. Lai, H. P. Yennawar and A. T. Radosevich, *J. Am. Chem. Soc.*, 2014, **136**, 17634–17644.
40 H. Kameo and H. Nakazawa, *Chem. Rec.*, 2017, **17**, 268–286.
41 J. M. Bayne and D. W. Stephan, *Chem. Soc. Rev.*, 2016, **45**, 765–774.
42 D. W. Stephan, *Angew. Chem., Int. Ed.*, 2017, **56**, 5984–5992.
43 D. You and F. P. Gabbai, *J. Am. Chem. Soc.*, 2017, **139**, 6843–6846.
44 J. S. Jones, C. R. Wade, M. Yang and F. P. Gabbai, *Dalton Trans.*, 2017, **46**, 5598–5604.
45 J. S. Jones and F. P. Gabbai, *Chem. - Eur. J.*, 2017, **23**, 1136–1144.
46 J. S. Jones and F. P. Gabbai, *Acc. Chem. Res.*, 2016, **49**, 857–867.
47 N. Tan, Y. Chen, S. Yin, R. Qiu, Y. Zhou and C. T. Au, *Curr. Org. Chem.*, 2012, **16**, 2462–2481.
48 G. He, O. Shynkaruk, M. W. Lui and E. Rivard, *Chem. Rev.*, 2014, **114**, 7815–7880.
49 C. I. Rat, C. Silvestru and H. J. Breunig, *Coord. Chem. Rev.*, 2013, **257**, 818–879.
50 R. M. Minyaev, T. N. Gribanova and V. I. Minkin, in *Hyperbonding and Hypercoordination in Main-Group Chemistry*, ed. J. Reedijk and K. Poeppelmeier, Comprehensive Inorganic Chemistry (II), Elsevier, Oxford, 2013, pp. 109–132.
51 G. Sean McGrady and J. W. Steed, Hypervalent Compounds Based in part on the article Indium: Inorganic Chemistry by Dennis G. Tuck which appeared in the Encyclopedia of Inorganic Chemistry, in *Encyclopedia of Inorganic Chemistry*, ed. R. B. King, R. H. Crabtree, C. M. Lukehart, D. A. Atwood and R. A. Scott, 1st edn, 2006, DOI: 10.1002/0470862106.ia094.
52 S. Sato, O. Takahashi and N. Furukawa, *Coord. Chem. Rev.*, 1998, **176**, 483–514.
53 R. Pajkert and G.-V. Roeschenthaler, *Organophosphorus Chem.*, 2013, **42**, 197–215.
54 K.-y. Akiba, M. Yamashita, Y. Yamamoto and S. Nagase, *J. Am. Chem. Soc.*, 1999, **121**, 10644–10645.

55 M. Yamashita, Y. Yamamoto, K. Akiba, D. Hashizume, F. Iwasaki, N. Takagi and S. Nagase, *J. Am. Chem. Soc.*, 2005, **127**, 4354–4371.
56 K.-y. Akiba, Y. Moriyama, M. Mizozoe, H. Inohara, T. Nishii, Y. Yamamoto, M. Minoura, D. Hashizume, F. Iwasaki, N. Takagi, K. Ishimura and S. Nagase, *J. Am. Chem. Soc.*, 2005, **127**, 5893–5901.
57 T. Yamaguchi, Y. Yamamoto, D. Kinoshita, K.-y. Akiba, Y. Zhang, C. A. Reed, D. Hashizume and F. Iwasaki, *J. Am. Chem. Soc.*, 2008, **130**, 6894–6895.
58 M. Yamashita, Y. Yamamoto, K.-y. Akiba and S. Nagase, *Angew. Chem., Int. Ed.*, 2000, **39**, 4055–4058.
59 J.-Y. Nakatsuji, Y. Moriyama, S. Matsukawa, Y. Yamamoto and K.-Y. Akiba, *Main Group Chem.*, 2007, **5**, 277–285.
60 N. Jun-ya and Y. Yohsuke, *Bull. Chem. Soc. Jpn.*, 2010, **83**, 767–776.
61 Y. Hirano, S. Kojima and Y. Yamamoto, *J. Org. Chem.*, 2011, **76**, 2123–2131.
62 H. Staudinger and J. Meyer, *Helv. Chim. Acta*, 1919, **2**, 619–635.
63 H. Staudinger and J. Meyer, *Helv. Chim. Acta*, 1919, **2**, 608–611.
64 W. Schlenk and J. Holtz, *Ber. Dtsch. Chem. Ges. B*, 1917, **50**, 274–275.
65 W. Schlenk and J. Holtz, *Ber. Dtsch. Chem. Ges. B*, 1916, **49**, 603–608.
66 D. Hellwinkel and H. Seifert, *Justus Liebigs Ann. Chem.*, 1972, **762**, 29–54.
67 G. Wittig and M.-H. Wetterling, *Justus Liebigs Ann. Chem.*, 1947, **557**, 193–201.
68 K. O. Christe, W. W. Wilson, G. J. Schrobilgen, R. V. Chirakal and G. A. Olah, *Inorg. Chem.*, 1988, **27**, 789–790.
69 R. W. Johnson and E. R. Holm, *J. Am. Chem. Soc.*, 1977, **99**, 8077–8078.
70 G. A. Olah, D. J. Donovan, J. Shen and G. Klopman, *J. Am. Chem. Soc.*, 1975, **97**, 3559–3561.
71 H. F. Bettinger, P. v. R. Schleyer and H. F. Schaefer, *J. Am. Chem. Soc.*, 1998, **120**, 11439–11448.
72 C. S. Ewig and J. R. Van Wazer, *J. Am. Chem. Soc.*, 1990, **112**, 109–114.
73 C. S. Ewig and J. R. Van Wazer, *J. Am. Chem. Soc.*, 1989, **111**, 4172–4178.
74 H. H. Michels and J. A. M. Jr., *J. Chem. Phys.*, 1990, **93**, 1805–1813.
75 I. V. Getmanskii and R. M. Minyaev, *J. Struct. Chem.*, 2008, **49**, 973–978.
76 D. Kurzydłowski and P. Zaleski-Ejgierd, *Sci. Rep.*, 2016, **6**, 36049.
77 A. R. Miller, R. R. Tsukimura and R. Velten, *Science*, 1967, **155**, 688.
78 I. J. Solomon, J. N. Keith and A. Snelson, *J. Fluorine Chem.*, 1972, **2**, 129–136.
79 A. Hasegawa, R. L. Hudson, O. Kikuchi, K. Nishikida and F. Williams, *J. Am. Chem. Soc.*, 1981, **103**, 3436–3440.
80 K. Nishikida and F. Williams, *J. Am. Chem. Soc.*, 1975, **97**, 7166–7168.
81 S. A. Shaffer, M. Sadílek and F. Tureček, *J. Org. Chem.*, 1996, **61**, 5234–5245.
82 F. Kiyokazu and T. Ryozo, *Bull. Chem. Soc. Jpn.*, 1995, **68**, 3309–3318.
83 V. Q. Nguyen, M. Sadilek, J. Ferrier, A. J. Frank and F. Tureček, *J. Phys. Chem. A*, 1997, **101**, 3789–3799.
84 R. W. Alder, A. G. Orpen and J. M. White, *J. Chem. Soc., Chem. Commum.*, 1985, 949–951.
85 F. Gerson, G. Gescheidt, U. Buser, E. Vogel, J. Lex, M. Zehnder and A. Riesen, *Angew. Chem., Int. Ed.*, 1989, **28**, 902–904.
86 F. Gerson, J. Knoebel, U. Buser, E. Vogel and M. Zehnder, *J. Am. Chem. Soc.*, 1986, **108**, 3781–3783.
87 L. Schneider, U. Englert and P. Paetzold, *Z. Anorg. Allg. Chem.*, 1994, **620**, 1191–1193.
88 M. Mueller, U. Englert and P. Paetzold, *Inorg.Chem.*, 1995, **34**, 5925–5926.
89 P. D. Livant, D. J. D. Northcott, Y. Shen and T. R. Webb, *J. Org. Chem.*, 2004, **69**, 6564–6571.
90 M. Yamashita, K. Kamura, Y. Yamamoto and K.-Y. Akiba, *Chem. - Eur. J.*, 2002, **8**, 2976–2979.
91 The solid-state molecular structure of $\mathbf{1^{Me}}$ is shown in ESI Fig. S5.† All cell parameters are listed in Table S5.†
92 P. Pyykkö and M. Atsumi, *Chem. - Eur. J.*, 2009, **15**, 186–197.
93 A. Bondi, *J. Phys. Chem.*, 1964, **68**, 441–451.
94 R. S. Rowland and R. Taylor, *J. Phys. Chem.*, 1996, **100**, 7384–7391.
95 J. K. Badenhoop and F. Weinhold, *J. Chem. Phys.*, 1997, **107**, 5422–5432.
96 S. S. Batsanov, *Inorg. Mater.*, 2001, **37**, 871–885.
97 M. Mantina, A. C. Chamberlin, R. Valero, C. J. Cramer and D. G. Truhlar, *J. Phys. Chem. A*, 2009, **113**, 5806–5812.
98 S. Alvarez, *Dalton Trans.*, 2013, **42**, 8617–8636.
99 The sum of N–O vdW values calculated based on crystallographic data ranges between 2.79 and 3.16 Å and that from pure theoretical methods ranges between 2.79 and 3.5 Å.
100 M. Shimizu and M. Nakatani, *Eur. J. Org. Chem.*, 2017, **2017**, 4695–4702.
101 Similar deviation was observed from calculations carried out using B3PW91/6-31G(d), UB3PW91/6-31G(d), and B3LYP/6-31G(d), UB3LYP/6-31G(d), and B3LYP/cc-pVDZ, UB3LYP/cc-pVDZ (see Fig. S7–S9†).
102 We also performed AIM analysis based on fully optimized geometries of **2** and **3**. Please see the ESI, Fig. S14 and Table S11.†
103 A. C. Tsipis, *Coord. Chem. Rev.*, 2017, **345**, 229–262.

